# ROBUST CONTROL FOR REUSABLE ROCKETS VIA STRUCTURED $H_\infty$ SYNTHESIS

**Marco Sagliano[1], Taro Tsukamoto[2], Ansgar Heidecker[1], José Macés Hernández[1], Stefano Farì[1], Markus Schlotterer[1], Svenja Woicke[1], David Seelbinder[1], Shinji Ishimoto[2], and Etienne Dumont[1]**

[(1)]*German Aerospace Center, Robert Hooke Str. 7, 28359, Bremen, Germany*
[(2)]*Japan Aerospace Exploration Agency, 7-44-1 Jindaiji Higashimachi, 182-8522, Chofu, Japan*

## ABSTRACT

This paper discusses the problem of synthesizing robust controllers for reusable rockets during the aerodynamic descent phase. Emphasis is given to a well-established subset of methods, specifically robust control techniques based on the $H_\infty$ concept. A thorough description of how this family of methods can be used for the descent phase of reusable rockets is provided, together with a comparison of the full- and structured-version of $H_\infty$ methods. The methodology, the problem faced and the performance that can be obtained are discussed. Some results are shown for CALLISTO, a reusable rocket demonstrator jointly developed by DLR, JAXA, and CNES.

## NOMENCLATURE

| | |
|---|---|
| $\delta_\phi$ | Roll Virtual deflection, rad |
| $\delta_\theta$ | Pitch Virtual deflection, rad |
| $\delta_\psi$ | Yaw Virtual deflection, rad |
| $D$ | Downrange, m |
| $C$ | Crossrange, m |
| $A$ | Altitude, m |
| $\mathbf{r}$ | position vector, m |
| $\mathbf{v}$ | velocity vector, m s$^{-1}$ |
| $\mathbf{a}^{grav}$ | gravity acceleration vector, m s$^{-2}$ |
| $\mathbf{a}^{thr}$ | thrust acceleration vector, m s$^{-2}$ |
| $\mathbf{a}^{aero}$ | aerodynamic acceleration vector, m s$^{-2}$ |
| $\mathbf{a}^{fict}$ | fictitious acceleration vector, m s$^{-2}$ |
| $\phi$ | roll angle with respect to $DCA$, rad |
| $\theta$ | pitch angle with respect to $DCA$, rad |
| $\psi$ | yaw angle with respect to $DCA$, rad |
| $p$ | angular rate around $x$ with respect to $DCA$ in body, rad s$^{-1}$ |
| $q$ | angular rate around $y$ with respect to $DCA$ in body, rad s$^{-1}$ |
| $r$ | angular rate around $z$ with respect to $DCA$ in body, rad s$^{-1}$ |
| $\omega$ | angular rate vector with respect to $DCA$ in body, rad s$^{-1}$ |
| $m$ | mass, kg |
| $\mathbf{I}$ | inertia, kg m$^2$ |
| $\mathbf{M}^{thr}$ | thrust torque vector, N m |
| $\mathbf{M}^{aero}$ | aerodynamic torque vector, N m |

| | |
|---|---|
| $\mathbf{M}^{RCS}$ | RCS torque vector, N m |
| $T_{vac}$ | Thrust in vacuum, N |
| $T$ | Thrust in atmosphere, N |
| $I_{sp}$ | specific impulse, s |
| $g_0$ | gravity acceleration at sea level, m s$^{-2}$ |
| $\mu_\oplus$ | Earth's gravitational parameter, m$^3$ s$^{-2}$ |
| $V$ | speed, m s$^{-1}$ |
| $\rho$ | atmospheric density, kg m$^{-3}$ |
| $A_{ref}$ | reference surface, m$^2$ |
| $L_{ref}$ | reference length, m |
| $\beta_1$ | first TVC deflection, rad |
| $\beta_2$ | second TVC deflection, rad |
| $C_x$ | Force aerodynamic coefficient along $x$ |
| $C_y$ | Force aerodynamic coefficient along $y$ |
| $C_z$ | Force aerodynamic coefficient along $z$ |
| $C_l$ | Torque aerodynamic coefficient around $x$ |
| $C_m$ | Torque aerodynamic coefficient around $y$ |
| $C_n$ | Torque aerodynamic coefficient around $z$ |

## 1 INTRODUCTION

The second decade of the new millennium has led to a complete disruption of the space sector, which has been shaken by the astonishing successes of SpaceX. The company led by Elon Musk has demonstrated that reusability is no longer a chimera pursued since the beginning of the Space Shuttle era, but a logical and technological step which is now at our hand [1]. Other companies like Blue Origin are following a similar path with the development of the reusable rockets New Shepard [2] and New Glenn [3]. This revolution could lead to an astronaut back to the Moon by 2024 and, even more ambitiously, to manned missions to Mars during the next 10 years.

To speed-up the pace of space-missions cost sustainability governmental agencies are now moving with decision towards the reusability paradigm. With this long-term vision in mind and the aim to develop strategic technologies in the frame of a wider reusability-focused program the German Aerospace Center (DLR), the Japan Aerospace Exploration Agency (JAXA), and the French National Centre for Space Studies (CNES) joined in a trilateral agreement to develop and demonstrate the technologies that will be needed for future reusable launch vehicles. In the joint project CALLISTO (Cooperative Action Leading to Launcher Innovation in Stage Toss back Operations) a demonstrator for a reusable vertical take-off, vertical landing rocket, acting as first stage, is developed and built. As long-term objective this project aims at paving the way to develop a rocket that can be reused, and the joint efforts of the three agencies will culminate in a demonstrator that will perform its first flights from the Kourou Space Center (KSC), in French Guiana.

Within the trilateral agreement two lines of development of G&C (Guidance and Control) subsystems take place in parallel for CALLISTO. Specifically, DLR and JAXA decided to strengthen their synergy and proceed with the development of a unique, fully integrated G&C subsystem. The missions consist of multiple flight phases, which correspond to different aerodynamic configurations of the vehicle. Specifically, four main phases of flight can be defined to better frame the problem: the ascent phase, the boostback maneuver, the aerodynamic phase, and the powered descent and landing phase. Therefore, a plethora of modern methods is needed to successfully and autonomously complete such an ambitious

mission. More specifically, one of the critical aspects to realize an ambitious program focused on reusability is the capability of the system to counteract disturbances and uncertainties acting on the vehicle while satisfying the strict accuracy requirements needed to realize pinpoint landing. Over the last decades several methodologies have been proposed to control vehicles during their atmospheric flight. Classic techniques involving Linear Quadratic Regulators were deeply exploited for winged systems [4, 5, 6]. This choice was motivated by the well-established heritage of these methods, and by the relative easiness of implementation and application to nonlinear systems, by applying gain-scheduling techniques based on linear interpolation.

An alternative approach based on nonlinear control was proposed to better address the intrinsic nonlinearity of the atmospheric entry dynamics (coming for example from aerodynamic and gravitational forces). In this case the idea was mainly to keep the dynamics in nonlinear form, but expressing in affine form with respect to the control. This reformulation of the problem leads to the possibility to implement dynamic-inversion-based techniques [7, 8, 9]. An interesting sub-methodology based on dynamic inversion is sliding-mode control, in its basic of high-order formulation, interesting because it removes chattering, a known limit of the basic version of this methods [10, 11]. These methods can be further robustified by including disturbance observers which reconstruct online disturbances or unmodeled effects perturbing the motion of the vehicle [12, 13]. Other interesting technologies which avoid gain-scheduling include model predictive control [14, 15, 16]. All of these methods have a common drawback: the control requirements can only be verified a posteriori via Monte-Carlo analysis.

A very elegant and appealing solution to this drawback is represented by the $H_\infty$ family of methods [17, 18]. These methods overcome the drawback in terms of classical stability margins of linear quadratic Gaussian (LQG) regulators, that is, to verbatim mention the abstract of Doyle [19], "'There are none"'. This deduction led therefore to the development of the $H_\infty$ framework for Linear-Time-Invariant (LTI) systems. The philosophy behind $H_\infty$ methods resides in the frequency-wise minimization of the maximum gain that a given output will experience for a unitary excitation of a generalized exogenous input. The control-plant interaction is modeled by using a lower Linear Fractional Transformation (LFT) representing the feedback action [20]. The approach has proven highly successfully and has gained popularity in both academia and industry as it allows to incorporate specific frequency-domain requirements in the design procedure by properly choosing weighting functions to emphasize a given objective within a specific range of frequencies (e.g., it is typically required to track well the reference signal at low frequencies, while having the system being insensitive to input noise). The entire synthesis process is nowadays highly automatized through the popular Matlab's *hinfsyn* routine [21]. This methodology has been so far affected by two main drawbacks: the former is that the controller itself is an LTI, whose size is at least as large as the size of the augmented plant itself. This leads to a rapid increase of the complexity of the synthesized controller, and to the need of applying ad-hoc reducing techniques, with in many cases a corresponding reduction of performance. The latter drawback is that the entire framework is intrinsically meant for LTI systems. Its application to nonlinear systems is not as straightforward as in the case of static-gain controllers, and while relevant progress in this sense have been made through the development of Linear Parameter-varying (LPV) techniques [22], still the methodology is not yet ready for handling general Linear Time Varying (LTV) systems.

The aforementioned drawbacks have been strongly mitigated by the second generation of $H_\infty$ methods, the so-called *structured* $H_\infty$ techniques [23]. The main difference with respect to the standard $H_\infty$ methodology resides in the fact that in the case of structured synthesis the designer can impose a specific control structure, like a Proportional-Integral-Derivative (PID) or a LTI system with a defined

number of states. This choice is translated into a set of constraints that leads to the definition of a non-smooth optimization problem, whereas in the original formulation the problem was convex. Despite the more complex mathematical framework, the procedure has been automatized and incorporated in the Matlab command *hinfstruct*, used throughout this work. The benefits of this new methodology is two-fold: first it allows to tune well-known controllers in $H_\infty$ sense, leading to the possibility to incorporate design requirements in the synthesis process exactly as done for standard $H_\infty$. Second, it allows to recover the possibility to use gain-scheduling techniques for those controllers having a static-gain nature, like Proportional-Derivative controllers. Finally, the trade-off between performance and complexity of the controller is no longer a result of a-posteriori reductions, but can be explored by the designer during the synthesis process, giving therefore a more transparent way to choose a given structure for a specific control problem.

In the space sector the aforementioned methodology has found significant applications in the launchers segment. It is a technology studied both in the United States the new Space Launch System, previously known as ARES-I [24, 25], and in Europe [26, 27, 28]. An interesting case is represented by the application of structured $H_\infty$ technique to the VEGA launcher, not only for synthesizing a robust controller, but also to retrieve through the same framework the baseline controller [29, 30, 31]. It is worth noticing that while this topic is getting more and more explored for the ascent phase, still, despite some remarkable exceptions [32] the properties of the same methodology for the descent phase of a reusable rocket remain unexplored.

This paper tries to reduce this lack by focusing on the feedback control strategy conceived for the aerodynamic descent of a reusable rocket. During this phase of the flight the fins are used to actively track the desired attitude, which will result in the desired aerodynamic forces required to track the trajectory computed by the guidance system. The controller needs to be extremely robust while satisfying the tight requirements of the mission.

This paper is organized as follows: In Sec. 2 we define the control problem for the aerodynamic descent phase. The formulation of the $H_\infty$ problem is formulated in Sec. 3, with the recovery of the baseline controller shown in Sec. 4. The new controllers are analyzed in Sec. 5, while the overall behavior of the resulting gain-scheduling controller is shown in Sec. 6. Finally, some conclusions regarding the work performed are drawn in Sec. 7.

## 2 PROBLEM STATEMENT

This section describes the motion of a reusable rocket during its aerodynamic descent phase. First the vehicle and the mission profiles are described. Then the specific control problem associated with the aerodynamic descent phase is described.

### 2.1 Vehicle and Mission Description

CALLISTO mounts an engine employing liquid hydrogen (LH2) and liquid oxygen (LOX) as propellants. The engine is able to generate a thrust in the order of 40 kN, with a throttling capability that can go down to 40%. Its height is about 13 m with a diameter of about 1 m. The engine is mounted on a gimballed system to allow to control the thrust vector pointing direction. During the active propulsion phases this guarantees full pitch and yaw control capability which is used for translational control. The roll control is realized mainly through a set of Reaction-Control thrusters which is installed at the top of the vehicle. During the non-propelled phases three-axes control is achieved through a set

of four aerodynamic fins which are mounted in a "+" configuration. Note that for what regards the control formulation the 4 fins can be mapped onto a set of *virtual deflections* $\delta_\phi$, $\delta_\theta$, $\delta_\psi$, which are used to express the aerodynamic coefficients, and therefore, are actively used for linearizing the equations of motion. Finally, the active landing system of CALLISTO is comprised of a set of 4 foldable legs. An impression of the vehicle is shown in Fig. 1.

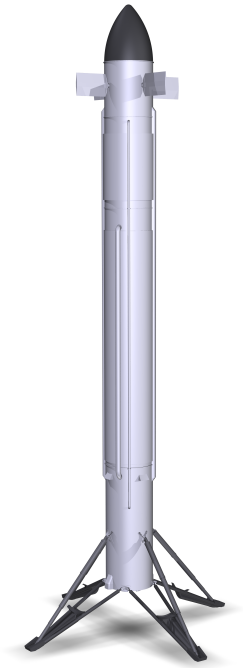

**Figure 1:** CALLISTO experimental vehicle

Note that whereas we refer to the CALLISTO demonstrator throughout this work the problem and the formulation can be considered applicable to any reusable rocket having a gimbaled engine, a set of fins for aerodynamic control and a set of RCS for roll control during the powered descent and landing phase. This broad range of vehicles can potentially include vehicles like SpaceX's Falcon 9 [33] and Blue Origin's New Shepard and New Glenn [3].

For what regards the mission profile the flight will take place in French Guiana, at the Kourou Space Center (GSC). After the ascent phase the vehicle starts its boostback maneuver to invert the direction of the velocity vector. After this maneuver is complete a MECO (Main Engine Cut Off) command is issued, and the vehicle starts its descent. As soon as the dynamic pressure is strong enough the actively controller aerodynamic descent phase begins. In this phase the attitude control is ensured by the fins that will steer the vehicle such that a given aerodynamic force, needed to track the trajectory, is generated. At about 2 km of altitude the engine is re-ignited and the powered descent and landing phase begins. The thrust force vector is used to control the translational motion of the vehicle. The attitude pitch and yaw motion is controlled by the TVC system, while the RCS provide roll control capabilities. Note that since a set of 8 RCS thrusters is mounted on CALLISTO, a more complex allocation / Pulse Width Modulation (PWM) algorithms are used. Nevertheless, it can be assumed as first approximation that the continuous roll torque computed by the controller can be delivered by the RCS thrusters, and no effects coming from PWM are taken into account. The trajectory can be observed in Fig. 2.

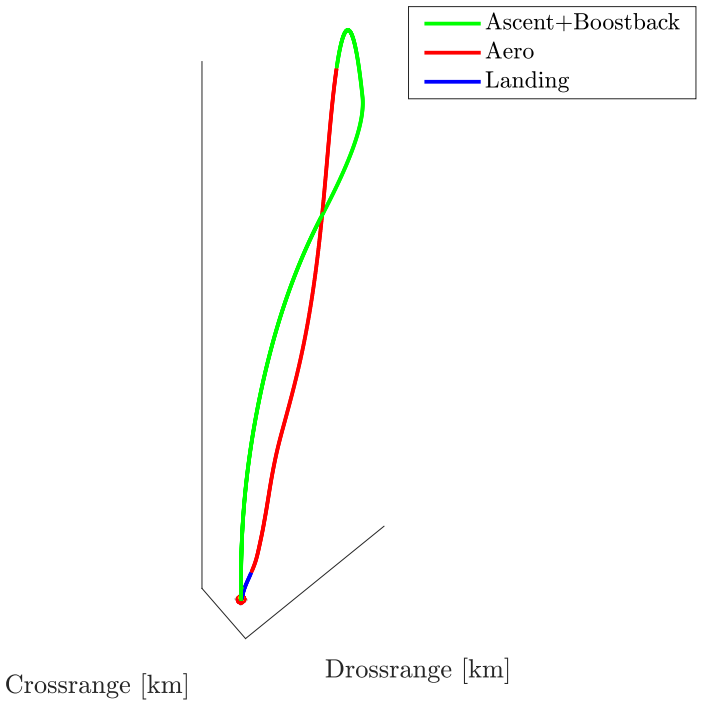


**Figure 2:** CALLISTO reference trajectory

### 2.2 6-DoF Equations of Motion

The mathematical description of the equations of motion relies upon a Downrange-Crossrange-Altitude (DCA) reference frame centered at the landing position. This choice helps the decoupling of the motion for both the translation and the rotation channels. The 6-DOF motion of a reusable rocket can be written as

$$\begin{aligned}
\dot{\mathbf{r}} &= \mathbf{v} \\
\dot{\mathbf{v}} &= \mathbf{a}^{grav} + \mathbf{a}^{thr} + \mathbf{a}^{aero} + \mathbf{a}^{fict} \\
\dot{\phi} &= p + (q\sin\phi + r\cos\phi)\tan\theta \\
\dot{\theta} &= q\cos\phi - r\sin\phi \\
\dot{\psi} &= (q\sin\phi + r\cos\phi)\cos\theta^{-1} \\
\dot{\omega} &= \mathbf{I}^{-1}\left(\mathbf{M}^{aero} + \mathbf{M}^{thr} + \mathbf{M}^{rcs} - \omega \times (\mathbf{I}\cdot\omega)\right) \\
\dot{m} &= -\frac{T_{vac}}{I_{sp} g_0}
\end{aligned} \tag{1}$$

where **r** and **v** are the position and velocity of the center of mass of the vehicle expressed in the DCA reference frame. The attitude is represented as a set of Euler angles, equal to 0 when the body axes are aligned with the Up, Crossrange and Downrange directions. This choice allows to avoid singularities when the vehicle is moving vertically, and is therefore a suitable solution for the descent and landing phase. The terms $\mathbf{a}^{grav}$ $\mathbf{a}^{thr}$, $\mathbf{a}^{aero}$ and $\mathbf{a}^{fict}$ represent the gravitational, propulsive, aerodynamic and fictitious accelerations acting on the rocket, respectively. They are computed as

$$
\begin{aligned}
\mathbf{a}^{grav} &= -\mu_{\oplus}\frac{\mathbf{r}+\mathbf{r_L}}{\|\mathbf{r}+\mathbf{r_L}\|^3} \\
\mathbf{a}^{thr} &= \mathbf{R}_B^{DCA}\cdot\frac{[T \quad 0 \quad 0]}{m} \\
\mathbf{a}^{aero} &= \mathbf{R}_B^{DCA}\cdot\tfrac{1}{2}\rho V^2 A_{ref}/m\,[C_x \quad C_y \quad C_z]^T \\
\mathbf{a}^{fict} &= -2\omega_{\oplus}\times\mathbf{v}-\omega_{\oplus}\times(\omega_{\oplus}\times\mathbf{r})
\end{aligned}
\tag{2}
$$

with the rotation matrix $\mathbf{R}_B^{DCA}$ representing the transformation from Body to the DCA axes and given by

$$
\mathbf{R}_B^{DCA} = \begin{bmatrix}
\cos\theta\cos\psi & \sin\phi\sin\theta\cos\psi-\cos\phi\sin\psi & \cos\phi\sin\theta\cos\psi+\sin\phi\sin\psi \\
\cos\theta\sin\psi & \sin\phi\sin\theta\sin\psi+\cos\phi\cos\theta & \cos\phi\sin\theta\sin\psi-\sin\phi\cos\psi \\
-\sin\theta & \sin\phi\cos\theta & \cos\phi\cos\theta
\end{bmatrix}
\tag{3}
$$

while the inverse transformation is computed by using the transpose of Eq. (3), since the inverse and the transpose of a rotation matrix coincide. The angular rates $\omega = [p \quad q \quad r]^T$ depend on the aerodynamic torque $\mathbf{M}^{aero}$, the propulsive torques $\mathbf{M}^{thr}$, and the torque provided by RCS $\mathbf{M}^{RCS}$:

$$
\begin{aligned}
\mathbf{M}^{aero} &= \tfrac{1}{2}\rho V^2 A_{ref} L_{ref}/m\,[C_l \quad C_m \quad C_n]^T \\
\mathbf{M}^{thr} &= (\mathbf{r}_{Thr}-\mathbf{r}_{CoM})\times[0 \quad -T\sin\beta_2 \quad T\sin\beta_1]^T \\
\mathbf{M}^{rcs} &= [M_\phi \quad 0 \quad 0]^T
\end{aligned}
\tag{4}
$$

The aerodynamic coefficients

$$
C_x, C_y, C_z, C_l, C_m, C_n \tag{5}
$$

refer to the body center of mass (CoM), and are function of Mach number $M$, angle of attack $\alpha$ (which embeds the attitude information) and fin deflections $\delta_\phi$, $\delta_\theta$ and $\delta_\psi$, while $\rho$ and $V$ refer to the atmospheric density and the speed, respectively. The same set of equations can be used for both the aerodynamic descent and the landing phase. The only difference is due to the fact that during the aerodynamic phase the vehicle will experience no thrust, and therefore the term $\mathbf{a}^{thr}$ will be 0 N. Moreover, we will rely only on the aerodynamic control capabilities of the rocket. Therefore the corresponding thrust and RCS torque contributions in terms of torque will be equal to 0 N m.

### 2.3 Aerodynamic Descent

During the aerodynamic descent we have to only rely on the aerodynamic forces and torques for the control of position and attitude, respectively. The overall control scheme is depicted in Fig. 3, where we can identify an outer loop and an inner loop. The outer loop is responsible of the trajectory tracking action. The physical means exploited to track the trajectory provided by the guidance system are in this phase the aerodynamic forces that are generated by the rocket due to its relative attitude with respect to the airflow. By commanding different pitch and yaw angles it is possible to generate the desired side forces which compensate for lateral error while descending. To successfully perform this action it is needed to ensure that the actual attitude of the rocket will follow the desired pitch and yaw profiles commanded by the outer loop. This action is responsibility of the inner loop that modifies the overall torque acting on the rocket by using the aerodynamic fins, and therefore changes its angular rate, and eventually its attitude.

Note that in Fig. 3 the navigation has been omitted. In the next sections we will show the results obtained by using the structured $H_\infty$ framework.

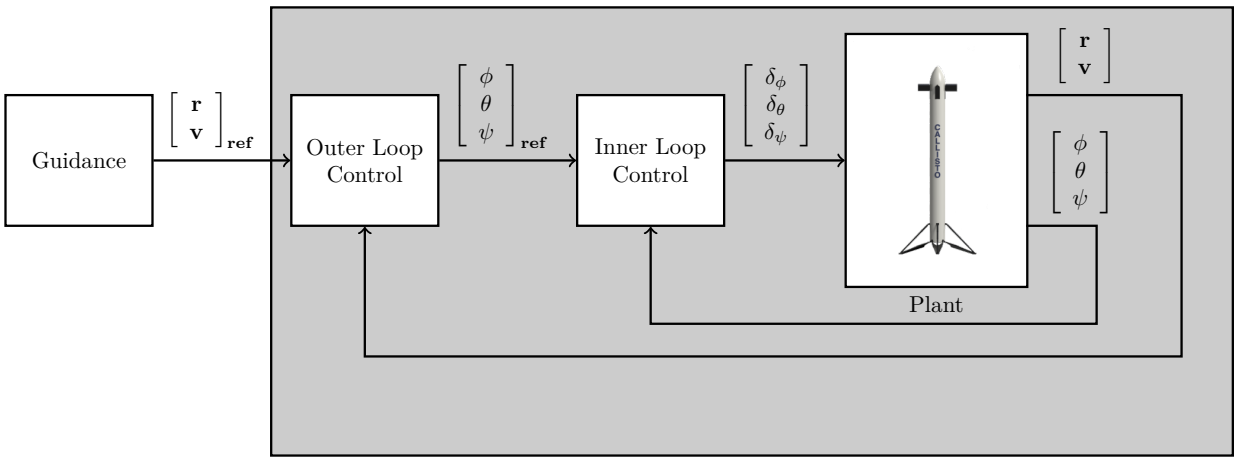


**Figure 3:** CALLISTO control loop for the aerodynamic descent

## 3 $H_\infty$ SYNTHESIS

The idea behind the structured $H_\infty$ control is to encapsulate the classical $H_\infty$ control within a given control template. In the classical $H_\infty$ theory a corresponding convex optimization problem is solved, and the result is the controller that will be a transfer function having at least the same order of the augmented plant to be controlled [34]. However, these controllers might have several problems. For instance they might be difficult to implement on a real system in case they present high-frequency poles. Moreover, the industrial adoption of controllers based on high-order transfer functions is generally more complicated. [31]. To overcome these problems Apkarian and Noll developed a framework based on non-smooth optimization to include constraints in the $H_\infty$ synthesis [35]. These constraints allow to impose a given control structure in the synthesis, for instance by imposing a classical Proportional-Integral-Derivative controller, which can be easily compared with baseline solutions. Moreover, all the validation techniques developed at industrial level for adopting these techniques can be directly applied to these $H_\infty$ controllers too, making much easier their wider understanding and development. In the context of CALLISTO we propose to couple this logic with the classical loop-separation documented in Fig. 3. Note that this choice is different from other formulations where the translational and rotational controls are combined within a unique framework [31], and different architectures are kept for future research. Here we propose separated decoupled controllers for roll, pitch, and yaw for what regards the attitude, and a fully integrated MIMO controller for downrange and crossrange position and velocity tracking. Results are validated by using both linear (e.g., in time domain and frequency domain) and non-linear (MonteCarlo numerical simulations) analysis. The procedure to derive the controller comprises the following steps:

1. Define a given number of controllers to be synthesized.
2. Choose a monotonically changing variable to be used as a scheduling parameter. For this work the altitude has been selected.
3. Sample the states of the reference solution along the scheduling parameter.
4. Perform a numerical linearization of the equations of motion of Eq. (1) to come up with a series of LTI systems
5. Perform a control synthesis and analysis for each of the LTIs obtained.
6. Analyze the individual linear controllers in both frequency and time domain.

7. Implement the gain-scheduling nonlinear controller by interpolating linearly the different gain matrices based on the current altitude.

For this work 10 different LTI systems have been heuristically selected.

### 3.1 Roll control

For the synthesis of roll control with the structured $H_\infty$framework we derived the following augmented plant $P$. We can observe the classical scheme with a reference signal $r$, scaled by a constant weighting function $W_{ref}$, which translates into a typical roll signal $\phi_{ref}$. At the same time we consider the presence of a noise signal $n$, scaled by $W_n$, that leads to a meaningful signal $n_\phi$ forming the measurement signal $\phi_m$. The comparison of $\phi_{ref}$ and $\phi_m$ provides the error $e_\phi$ that enters the controller $K$. The outcome is the roll-related deflection command $\delta_{\phi,cmd}$, which becomes the true deflection $\delta_\phi$ through the actuator transfer function $Act$. This is the signal that physically interacts with the plant $G_\phi$. For the tuning of the system we used a classical mixed $S/KS$ sensitivity approach, where the sensitivity transfer function $S$ is bounded by the inverse of $W_s$, while the control transfer function $KS$, measuring the control effort, is frequency-wise bounded by $W_u^{-1}$.

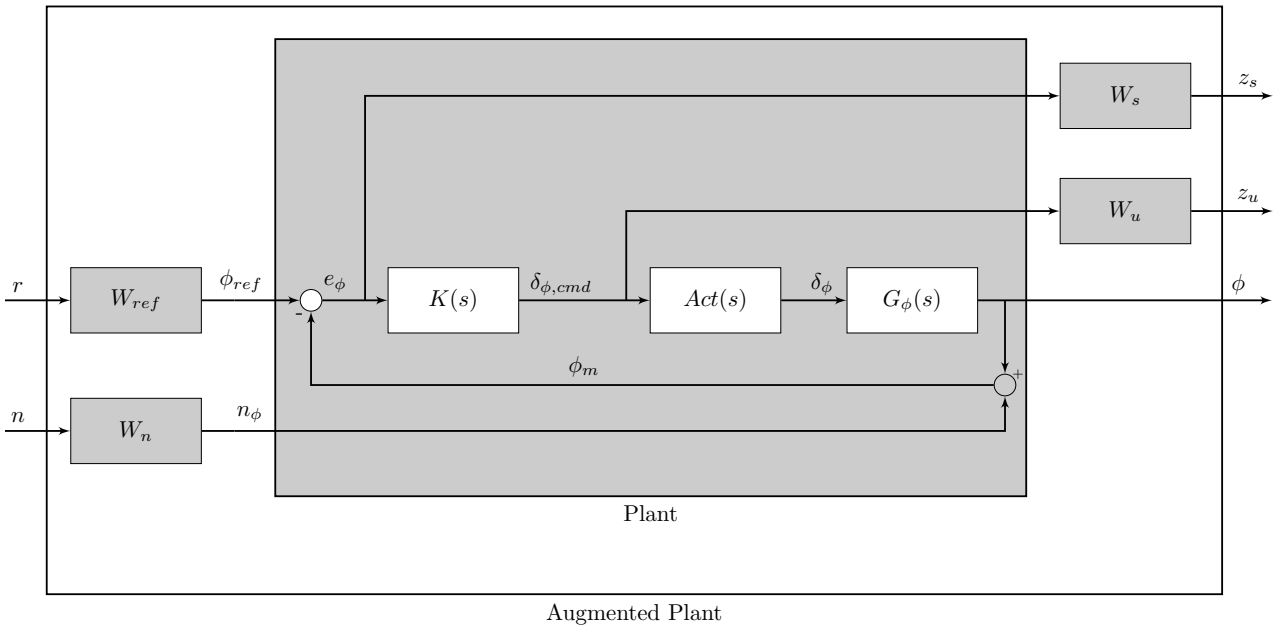


**Figure 4:** Roll Control augmented plant

The purpose of the optimization is therefore to minimize $\gamma$ as follows.

$$\underset{K \triangleq PID(s)}{\text{minimize}}\ \gamma = \left\| P_{\mathbf{r}\to\mathbf{z}(s)} \right\|_\infty \tag{6}$$

where the vectors **r** and **z** are the following.

$$\mathbf{r} \triangleq \begin{bmatrix} r \\ n \end{bmatrix}, \quad \mathbf{z} \triangleq \begin{bmatrix} z_s \\ z_u \end{bmatrix} \tag{7}$$

We are therefore finding the gains $K_p$, $K_d$, $K_i$ associated with a PID control structure which minimize the $\infty$-norm of the transfer function from **r** to **z** while stabilizing the closed loop.

### 3.2 Pitch and Yaw control

The same process is repeated for pitch and yaw (and here depicted only for the pitch dynamics, given the strong similarity of yaw results). The adopted scheme is depicted in Fig. 5.

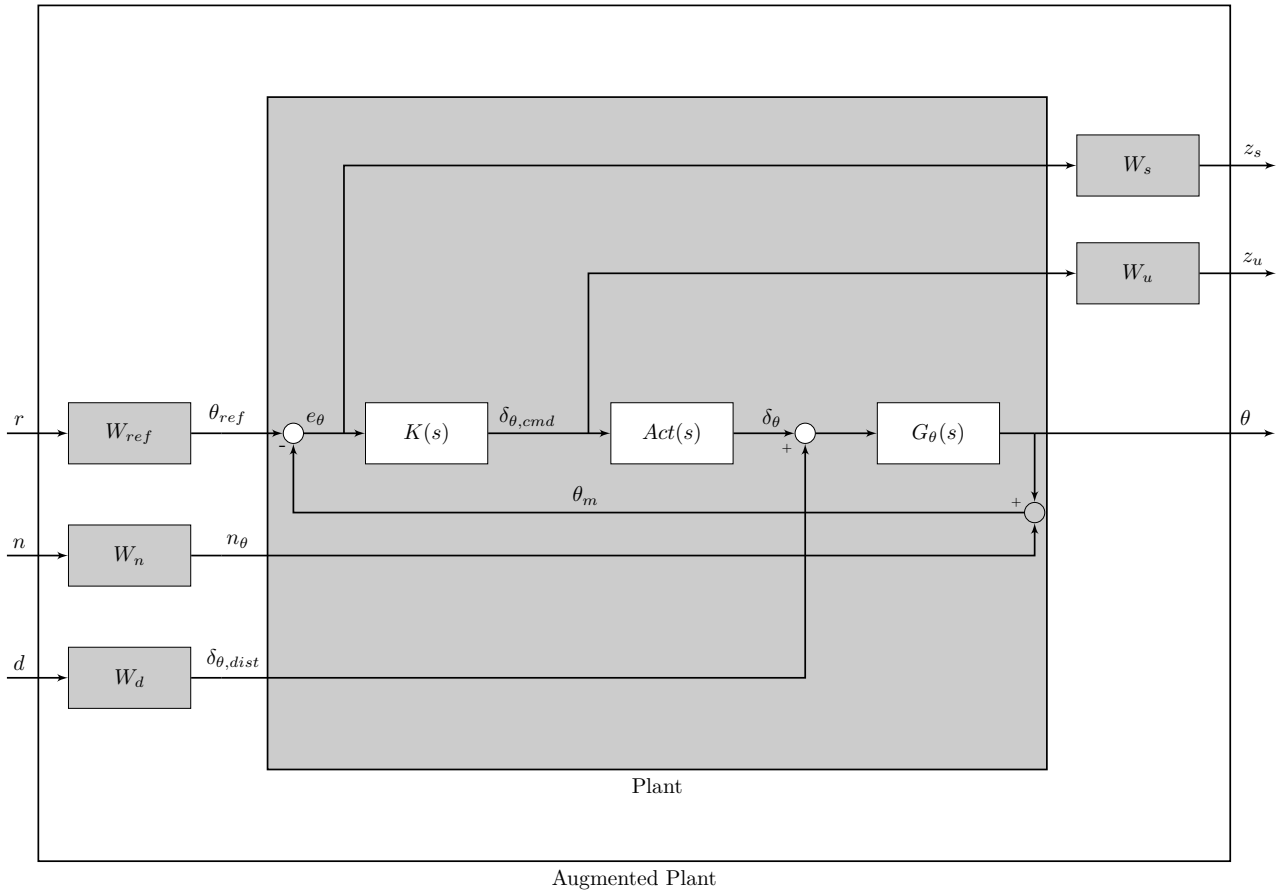


**Figure 5:** Pitch Control augmented plant

The main difference with respect to the roll is the presence of a further term $d$, representing the disturbances acting on the system at input level. In fact, this unitary signal is scaled by a constant function $W_d$, representing the magnitude of the real disturbances $\delta_{\theta,dist}$, which will modify the real deflection $\delta_\theta$ generated by the actuator, leading to the final value $\delta_\theta$. This modification to the design has been included to avoid zero-pole cancellation occurring on the pitch channel [36], while the remaining part of the augmented plant is similar to its roll counterpart. We are interested to synthesize a controller as follows.

$$\underset{K \triangleq PID(s)}{\text{minimize}} \; \gamma = \left\| P_{\mathbf{r} \to \mathbf{z}(s)} \right\|_\infty \tag{8}$$

where the vectors **r** and **z** are now defined as follows.

$$\mathbf{r} \triangleq \begin{bmatrix} r \\ n \\ d \end{bmatrix}, \quad \mathbf{z} \triangleq \begin{bmatrix} z_s \\ z_u \end{bmatrix} \tag{9}$$

Note that, as aforementioned, for the yaw control the same process as for the pitch has been implemented. Therefore, the scheme is here omitted for avoiding redundant information.

### 3.3 Trajectory tracking control

For what regards the trajectory tracking controller we propose to directly formulate the problem in a MIMO fashion as depicted in Fig. 6.

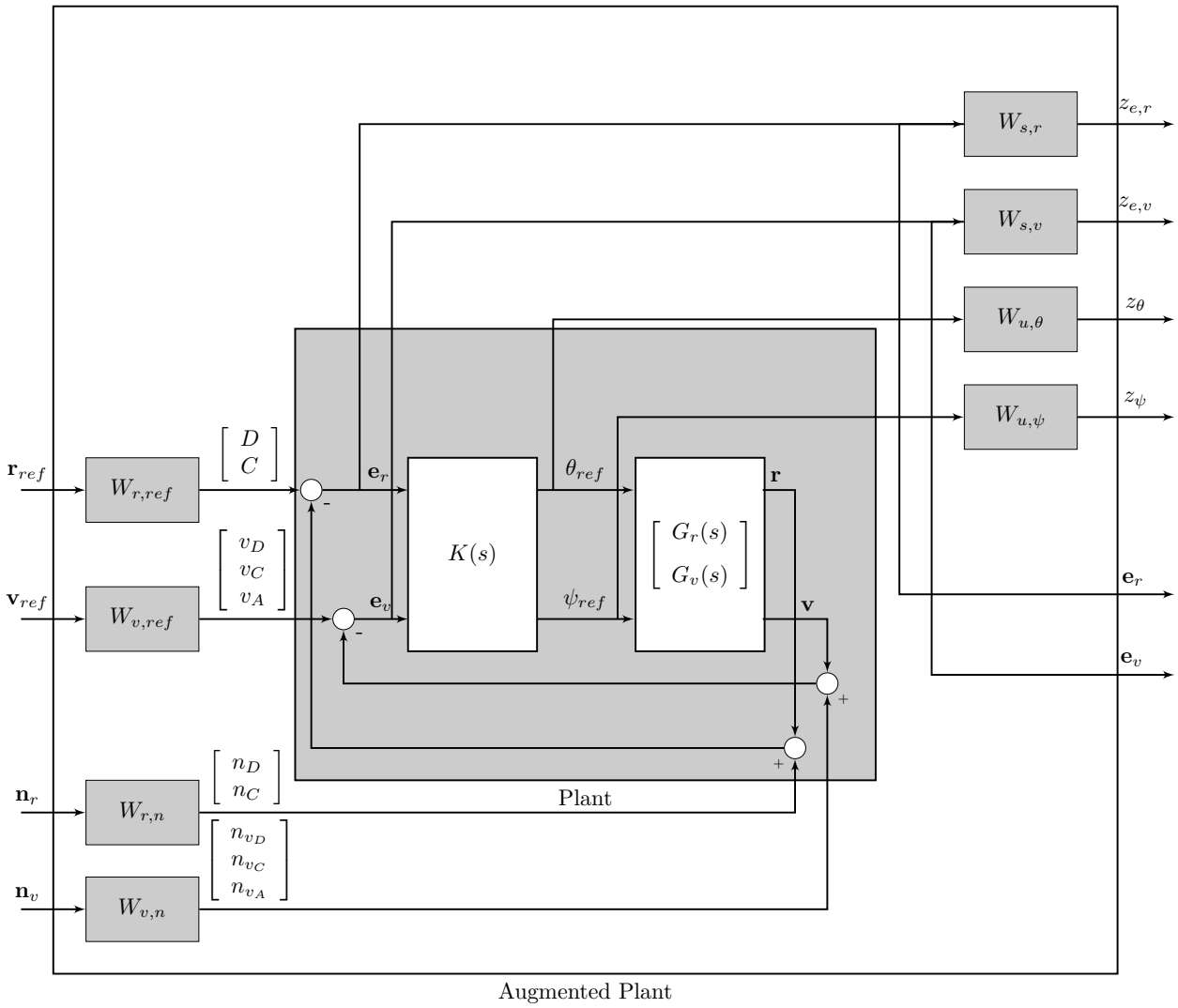


**Figure 6:** Trajectory Tracking control augmented plant

In this case we can see the reference position and velocity vectors $\mathbf{r}_{ref}$ $\mathbf{v}_{ref}$ (expressed in downrange-crossrange-altitude) scaled by the corresponding constant transfer function $W_{r,ref}$ and $W_{v,ref}$. The same process is applied to the noise signals $\mathbf{n}_r$ and $\mathbf{n}_v$, which are combined with the actual position $\mathbf{r}$ and velocity $\mathbf{v}$ to get the errors $\mathbf{e}_r$ and $\mathbf{e}_v$. These signals enter the MIMO controller $K(s)$, which computes the attitude commands $\theta_{ref}$ and $\psi_{ref}$ to be sent to the outer loop plant, representing the translational dynamics during the aerodynamic descent. Finally, sensitivity transfer functions are penalized through the weighting functions $W_{s,r}^{-1}$ and $W_{s,v}^{-1}$, whereas the control sensitivity transfer functions are bounded by $W_{u,\theta}$ and $W_{u,\psi}$, respectively. Note that since the altitude is the scheduling parameter it is not included in the feedback design, since it will be satisfied by definition, while the altitude rate is taken into account. For what regards the control structure we imposed in this case an LQR-like structure, essentially embedded in the matrix $K$,

$$K = \begin{bmatrix} k_{\theta,D} & k_{\theta,C} & k_{\theta,v_D} & k_{\theta,v_C} & k_{\theta,v_A} \\ k_{\psi,D} & k_{\psi,C} & k_{\psi,v_D} & k_{\psi,v_C} & k_{\psi,v_A} \end{bmatrix} \tag{10}$$

which in essence represents a MIMO Proportional-Derivative (PD) Controller. The corresponding control synthesis problem is therefore defined as follows.

$$\underset{K \triangleq LQR(s)}{\text{minimize}}\ \gamma = \left\| P_{\mathbf{r}\to\mathbf{z}(s)} \right\|_\infty \tag{11}$$

where the vectors **r** and **z** are accordingly defined as follows.

$$\begin{aligned} \mathbf{r} &\triangleq \begin{bmatrix} D & C & V_D & V_C & V_A & n_D & n_C & n_{v_D} & n_{v_C} & n_{v_A} \end{bmatrix}^T \\ \mathbf{z} &\triangleq \begin{bmatrix} z_D & z_C & z_{v_D} & z_{v_C} & z_{v_A} & z_\theta & z_\psi \end{bmatrix}^T \end{aligned} \tag{12}$$

## 4 BASELINE RECOVERY

To first get acquainted with the capabilities of the framework proposed in Sec. 3 we use it to reconstruct previously defined baseline attitude controllers, based on the same structures, but manually tuned. This exercise, performed in the same spirit of what proposed by Navarro-Tapia et Al. [30], has two benefits. First, since the gains (and consequently the frequency- and time-domain analyses) of the derived controllers are very close to the baseline controllers, the recovery of the baseline controllers confirms the consistency of the entire toolchain. Second, this activity provides a starting point for tuning the robust version of the controllers. Figs. 7 and 8 show the time responses for roll and pitch, respectively, whereas the corresponding information in frequency domain are shown in Figs. 9 and 10.

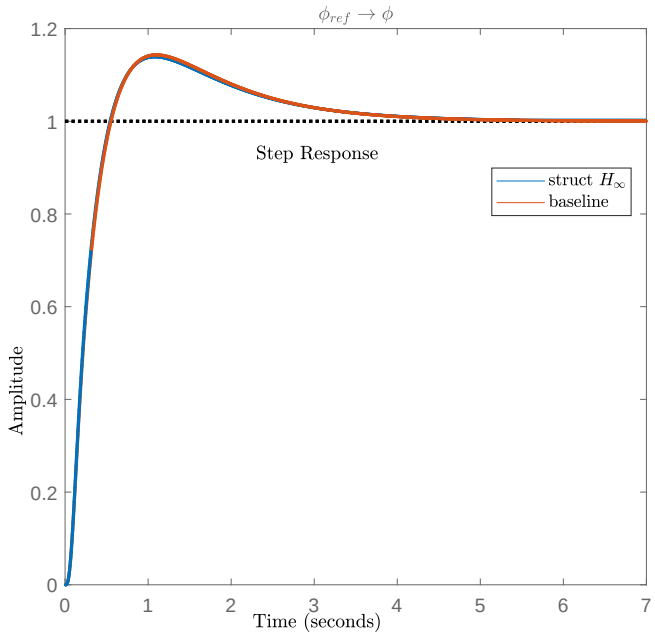


**Figure 7:** Recovery of baseline roll control: time domain comparison

From the plots it is visible how the structured $H_\infty$framework is able to successfully reconstruct the baseline controller. In fact, the observed discrepancy in the gains is less than 1% for both roll and

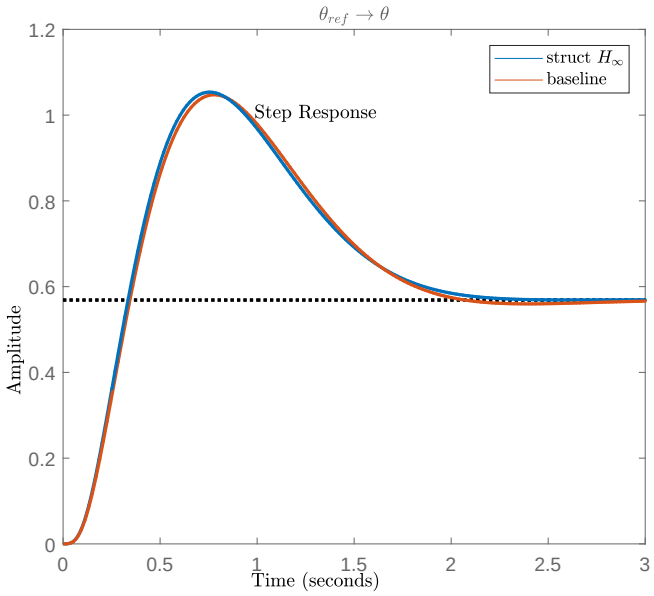


**Figure 8:** Recovery of baseline pitch control: time domain comparison

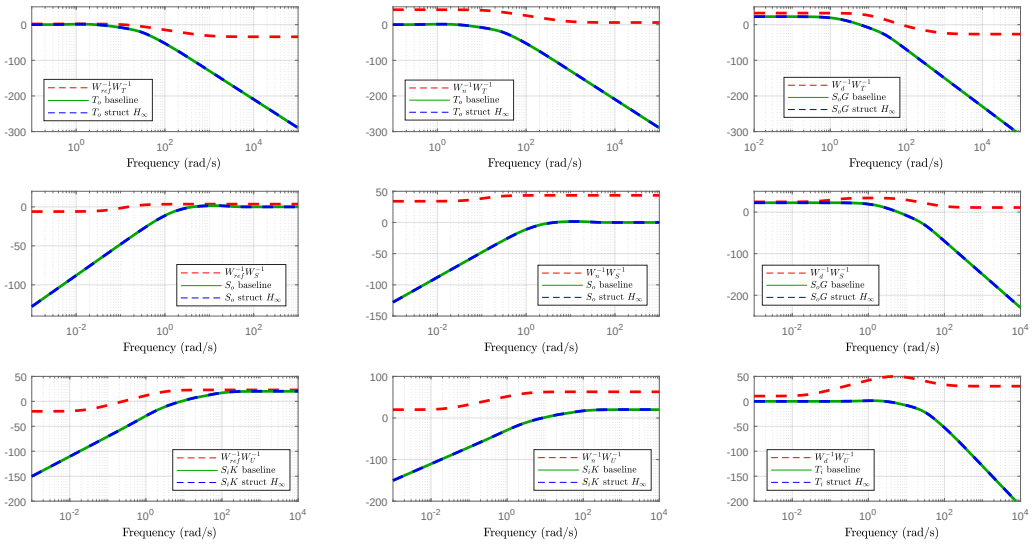


**Figure 9:** Recovery of baseline roll control: frequency domain comparison

pitch/yaw controllers, and therefore the reconstruction of the baseline controller is considered satisfactory. Note that this reconstruction was performed for a different mission scenario. A major scenario update occurred after this activity was completed, and since the purpose of its implementation was at that stage already fulfilled, the reconstruction was not performed for the new scenario. Finally, note that the baseline controller showed poor performance (as visible especially in Fig. 8), but this aspect was not a problem, since it was essentially only derived as first hand-made guess to have stable closed-loop with no emphasis on performance, since the following adoption of the structured $H_\infty$was already planned.

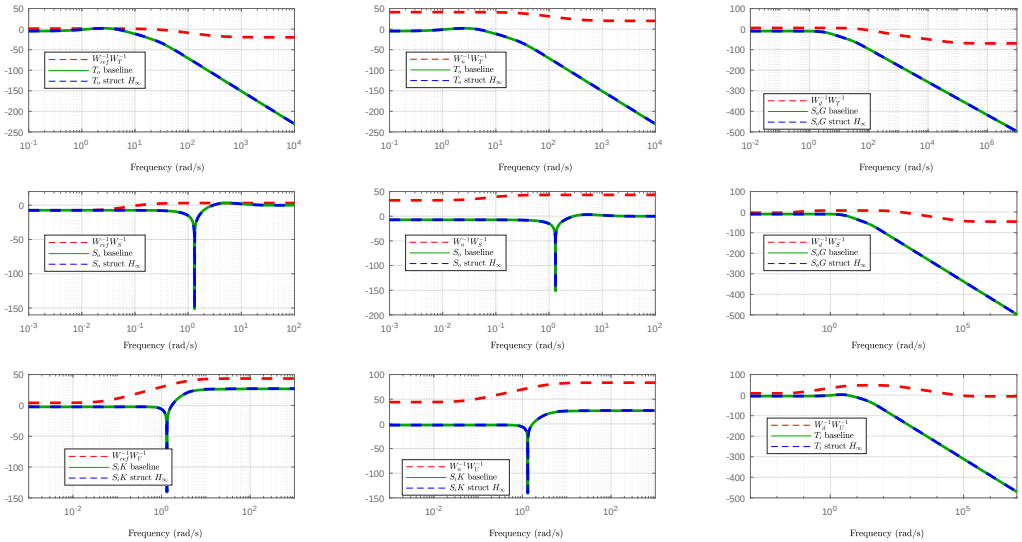


**Figure 10:** Recovery of baseline pitch control: frequency domain comparison

## 5 LINEAR ANALYSIS

After the baseline reconstruction was complete, it has been possible to perform a new tuning to get better performance and stability of the controllers for the new scenario. In fact, even though the previous reconstruction was satisfactory relative to the comparison with the baseline controller, the absolute performance of the baseline controller (and therefore of the reconstructed structured $H_\infty$controller version) was not very good. For example the steady-state error of the pitch controller was quite big, and if we looked at the stability margins, they were not very large either. For these reasons a brand new tuning by using the same framework was performed, and the results are summarized in Figs. 11 through 14, depicting again the time and frequency domain for both roll and pitch/yaw controllers, as well as for the outer loop (Figs. 15 and 16). Note that every time a structured $H_\infty$controller is derived, its corresponding full version is synthesized as well to directly have a measaure of the trade-off coming from adopting a specific structure. The attitude results show good performance, visible both in frequency and time domain. The complementary sensitivity function and the sensitivity function for the angles do not show peaks, indicating therefore good gain and phase stability margins (above 6 dB and 30 ° in nominal conditions). The structured and the full controllers are quite close to each other in terms of performance, confirming that the chosen PID template is sufficient to satisfy the control requirements. The same conclusions can be drawn for the pitch and yaw controllers. For what regards the MIMO controller (Figs. 15 and 16) we can observe a lack of peaks as well, and stability margins above the requirements. Moreover, from the step response analysis of Fig. 16 we can observe that the controller achieves a very good decoupling between the crossrange and the downrange axes. Finally, note that, even if not visible in the results for confidentiality reasons, the two control strategies implemented for attitude and trajectory have a separation of about one decade in frequency for what regards their closed-loop bandwidth, making the assumption of using a cascade control strategy valid.

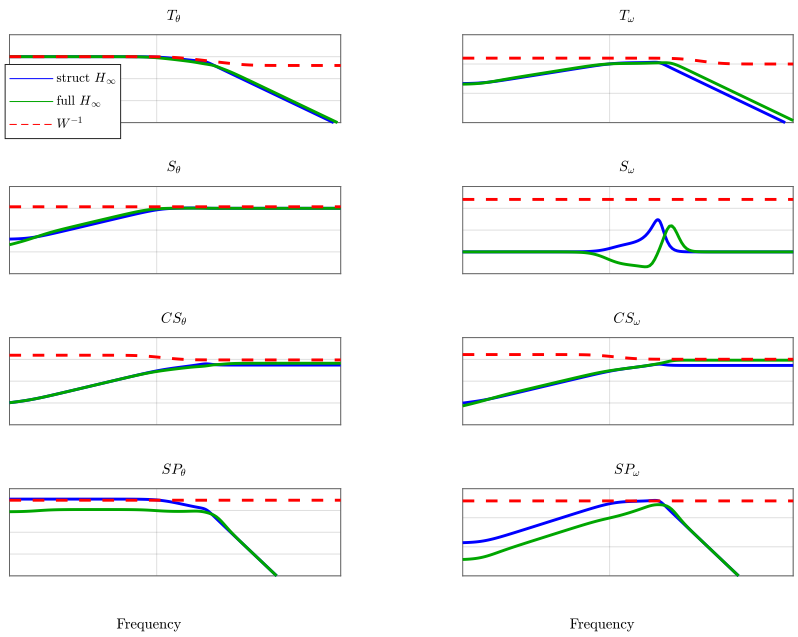


**Figure 11:** Design of a single roll controller: frequency domain

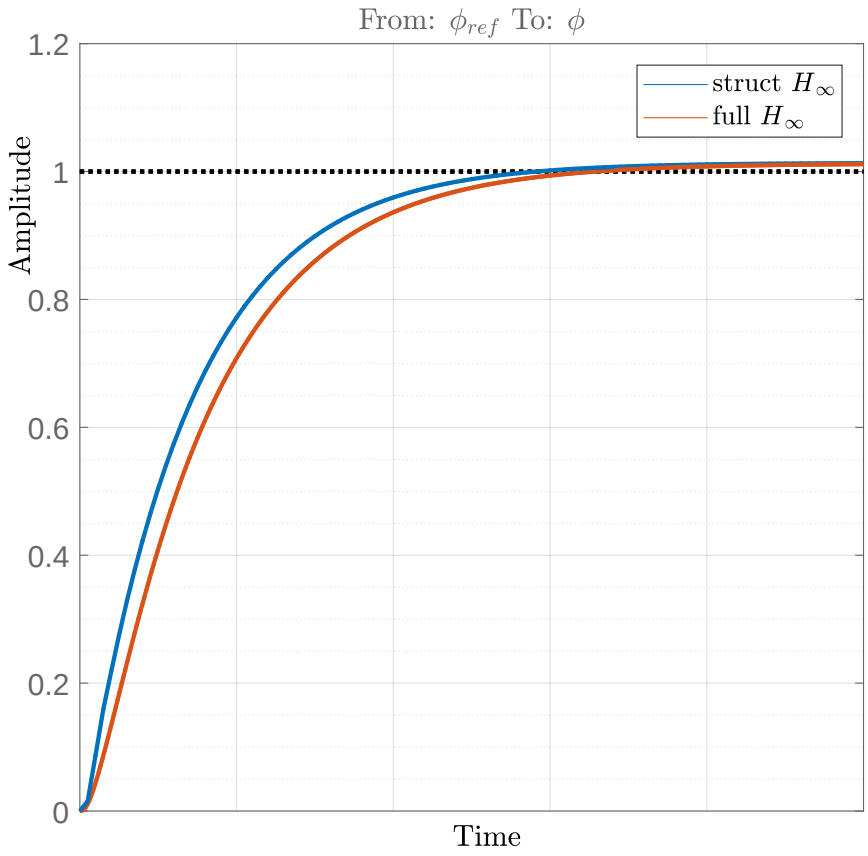


**Figure 12:** Design of a single roll controller: time domain analysis

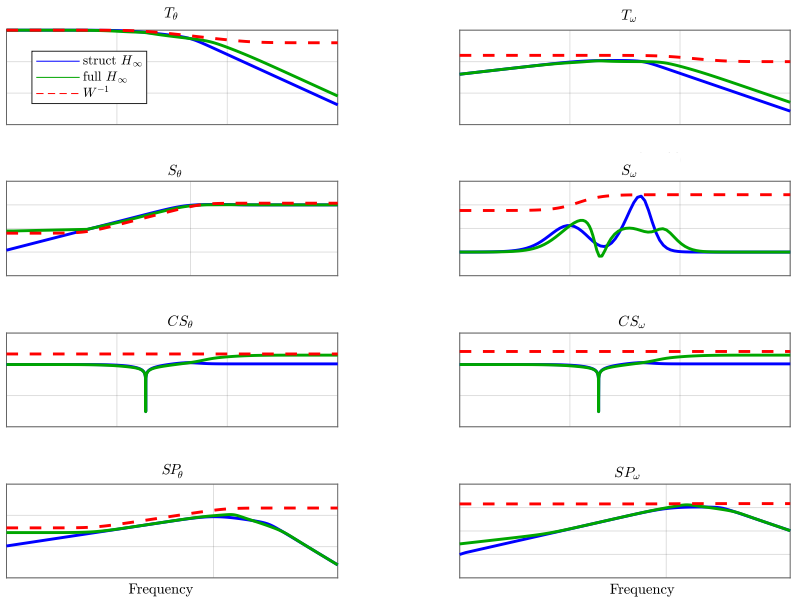


**Figure 13:** Design of a single pitch controller: frequency domain

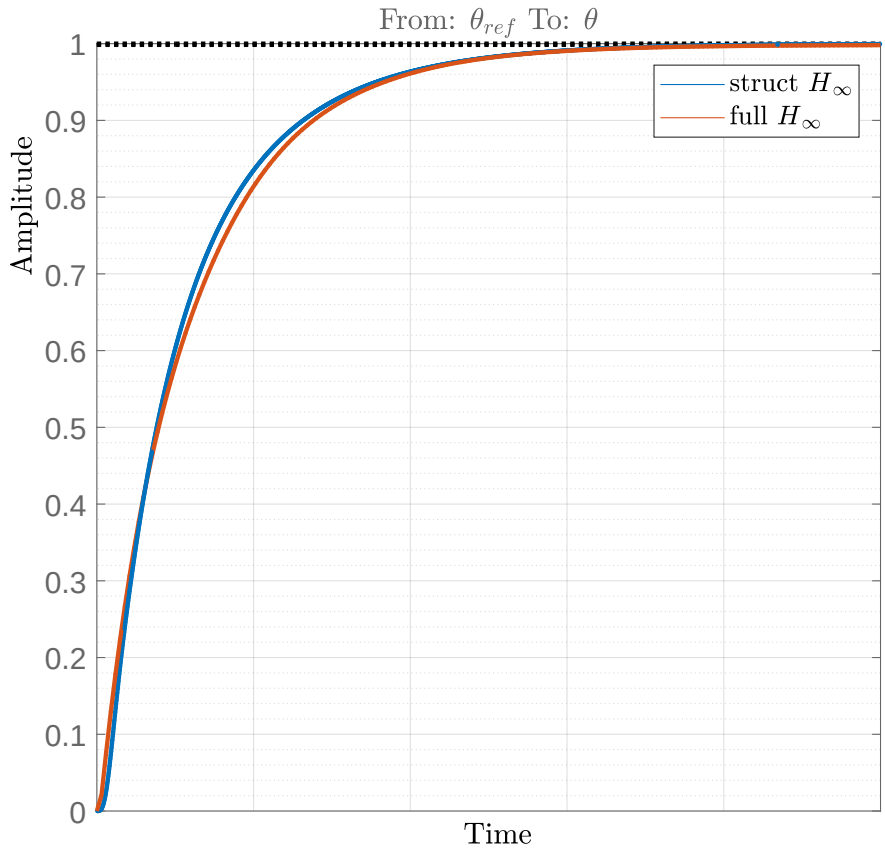


**Figure 14:** Design of a single pitch controller: time domain analysis

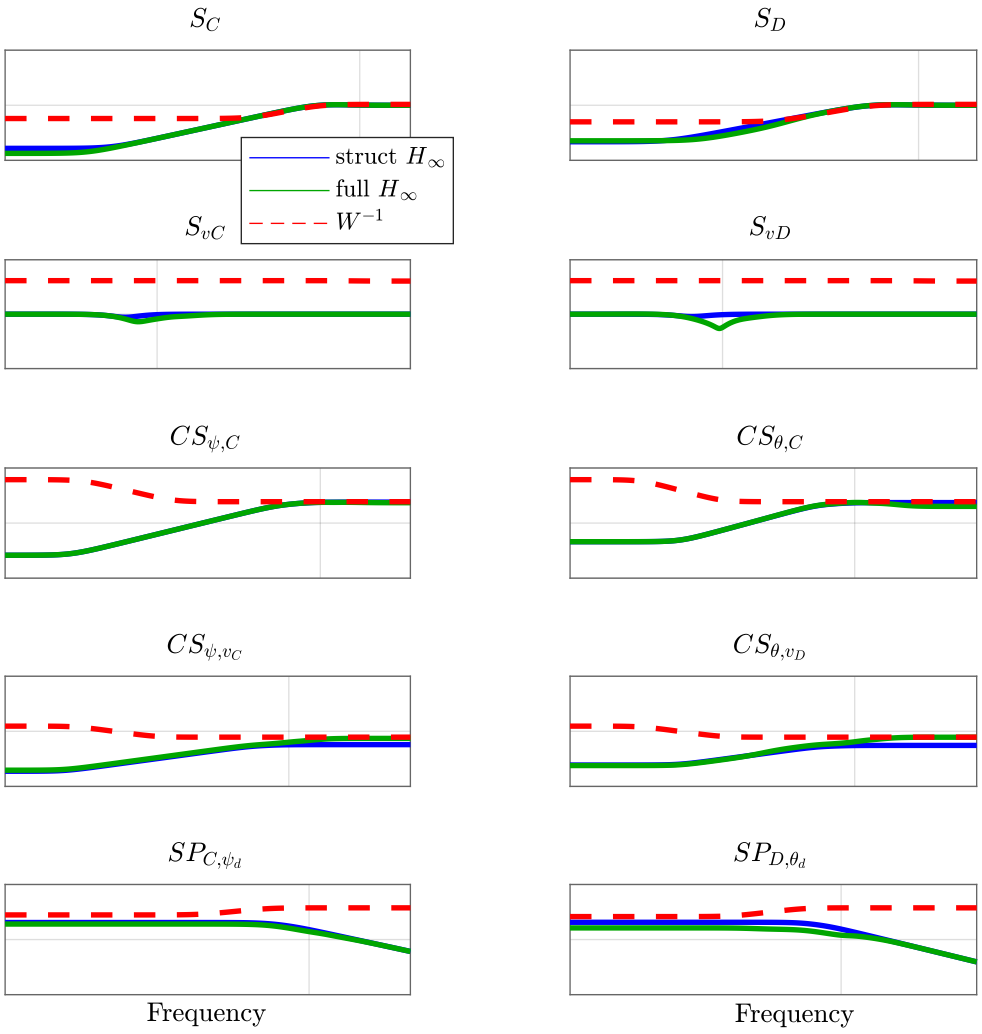


**Figure 15:** Design of a single outer loop controller: frequency domain

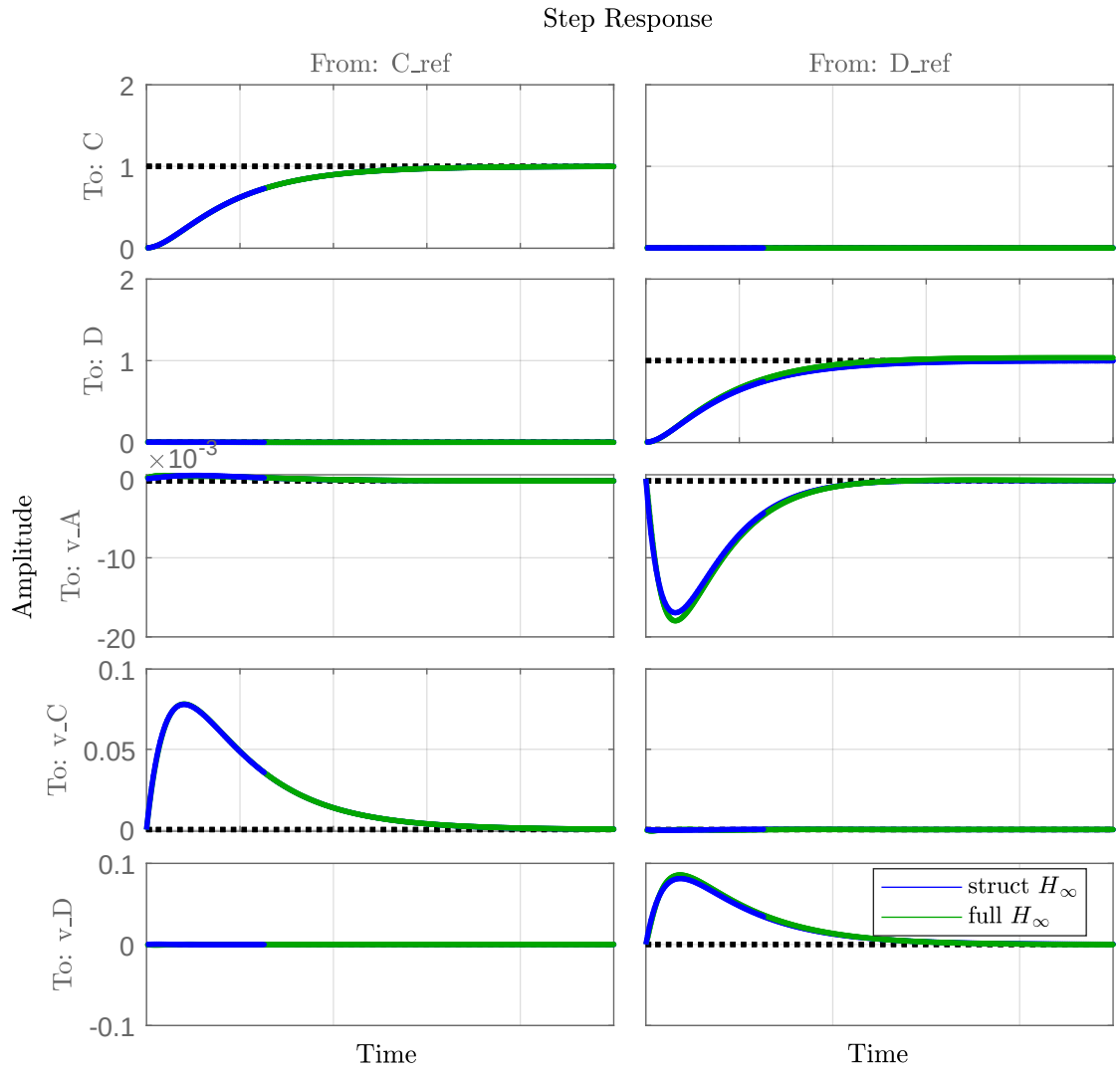


**Figure 16:** Design of a single outer loop controller: time domain analysis

## 6 NONLINEAR SIMULATIONS

In this section some results coming from a campaign of nonlinear simulations are described. In total a preliminary campaign of 200 cases has been run. This campaign includes dispersions on vehicle's properties, like mass, thrust, aerodynamic coefficients, as well as on environmental properties, including the atmospheric variables, and different wind profiles. Results in terms of attitude and position errors are depicted in Figs. 17 and 18, while the resulting closed-loop trajectories are depicted in Fig. 19.

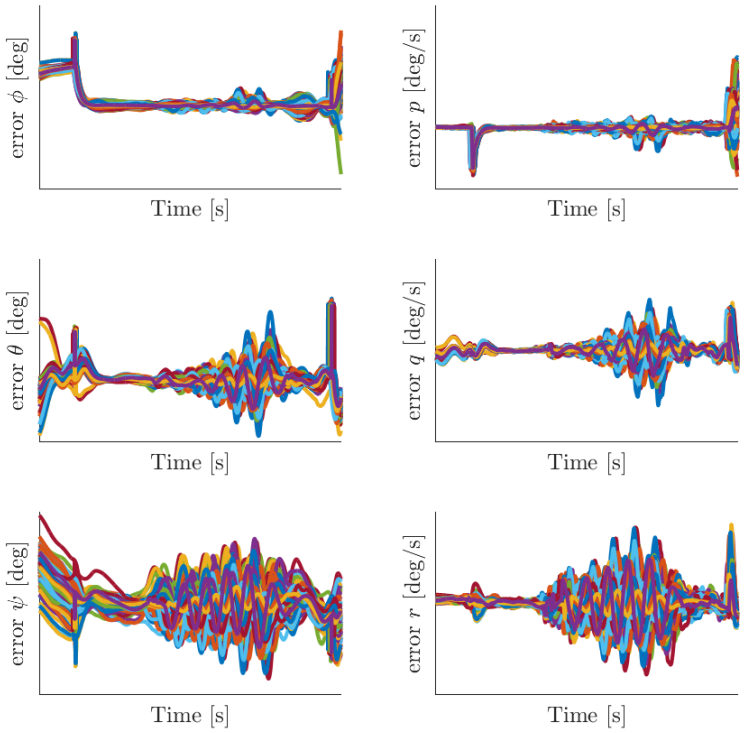


**Figure 17:** MonteCarlo campaign - attitude error profiles

All the cases are stable. Oscillations, visible especially in the pitch and yaw angle profiles, are within the prescribed bounds, even though we expect to further reduce them with the inclusion of uncertainties in the control synthesis framework. Nevertheless, the actual errors in terms of position and velocity (Fig. 18 are within the prescribed bounds as well. The resulting closed-loop trajectories depicted in Fig. 19 clearly show how the aerodynamic control strategy is able to manage the error and reduce the dispersion along the descent segment of the trajectory.

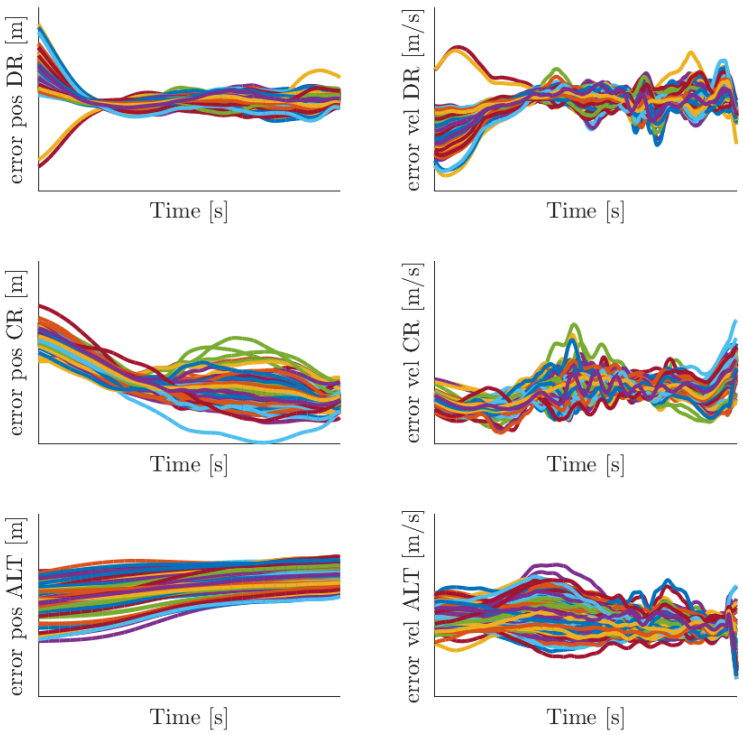


**Figure 18:** MonteCarlo campaign - position error profiles

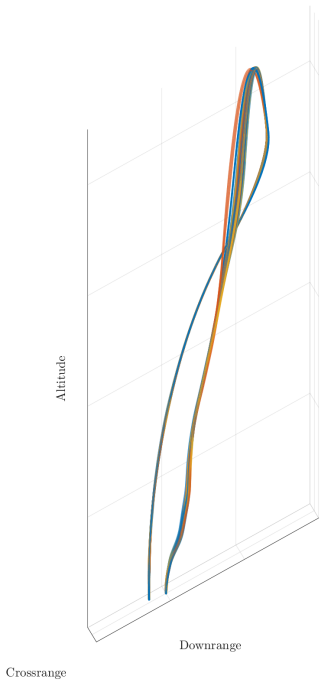


**Figure 19:** MonteCarlo campaign - 6-DoF closed-loop trajectories

## 7 CONCLUSIONS

In this paper we discussed the use of structured $H_\infty$controllers applied to the aerodynamic descent of a reusable rocket. The $H_\infty$framework has bee applied to a classical outer loop / inner loop cascade control design, and the same framework has been previously used to retrieve the pre-existing baseline controller, confirming its capability to move from basic PID controllers to a full $H_\infty$synthesis. This versatility provides large room for trade-offs in terms of control structure complexity and performance of the controller to the designer, opening up new possibilities for the application of this technique to high-demanding scenarios such as the ones associated with reusable rockets. Linear analysis in both time and frequency domain, and nonlinear analysis coming from a preliminary Monte-Carlo campaign confirm the validity of the proposed approach to the problem of interest.

Further development will include a thorough robustness analysis based on the use of linear fractional transformations. Moreover, we foresee to perform a comparison of the control synthesis framework presented here with an alternative one able to directly synthesize a unified 6-DoF control strategy, and to assess a difference in terms of nominal and robust stability and performance.

## REFERENCES


[1] space.com. *Wow! SpaceX Lands Orbital Rocket Successfully in Historic First*. Retrieval Date: 09-Mar-2020. 2015. URL: http://www.space.com/31420-spacex-rocket-landing-success.html.

[2] space.com. *Blue Origin Makes Historic Reusable Rocket Landing in Epic Test Flight*. Retrieval Date: 09-Mar-2020. URL: http://www.space.com/31202-blue-origin-historic-private-rocket-landing.html.

[3] arstechnica.com. *Blue Origin releases details of its monster orbital rocket*. Retrieval Date: 09-Mar-2020. URL: https://arstechnica.com/science/2017/03/blue-origin-releases-details-of-its-monster-orbital-rocket/.

[4] Axel Roenneke and Klaus Well. "Reentry control of a low-lift maneuverable spacecraft". In: *Guidance, Navigation and Control Conference*. American Institute of Aeronautics and Astronautics, Aug. 1992. DOI: 10.2514/6.1992-4455.

[5] Axel Roenneke and Abert Markl. "Reentry control to a drag vs. energy profile". In: *Guidance, Navigation and Control Conference*. American Institute of Aeronautics and Astronautics, Aug. 1993. DOI: 10.2514/6.1993-3790.

[6] E. Mooij. *Linear Quadratic Regulator Design for an Unpowered, Winged Re-Entry Vehicle (Series 08 - Astrodynamics and Satellite Systems , No 3)*. Delft Univ Pr, 1998. ISBN: 9040715971.

[7] Axel Roenneke and Klaus Well. "Nonlinear flight control for a high-lift reentry vehicle". In: *Guidance, Navigation, and Control Conference*. American Institute of Aeronautics and Astronautics, Aug. 1995. DOI: 10.2514/6.1995-3370.

[8] Sanjay Bharadwaj et al. "Tracking law for a new entry guidance concept". In: *22nd Atmospheric Flight Mechanics Conference*. American Institute of Aeronautics and Astronautics, Aug. 1997. DOI: 10.2514/6.1997-3581.

[9] Joel Benito and Kenneth Mease. "Nonlinear Predictive Controller for Drag Tracking in Entry Guidance". In: *AIAA/AAS Astrodynamics Specialist Conference and Exhibit*. American Institute of Aeronautics and Astronautics, Aug. 2008. DOI: 10.2514/6.2008-7350.

[10] Charles E. Hall and Yuri B. Shtessel. “Sliding Mode Disturbance Observer-Based Control for a Reusable Launch Vehicle”. In: *Journal of Guidance, Control, and Dynamics* 29.6 (Nov. 2006), pp. 1315–1328. DOI: 10.2514/1.20151.

[11] Roberto Furfaro and Daniel Wibben. “Mars Atmospheric Entry Guidance via Multiple Sliding Surface Guidance for Reference Trajectory Tracking”. In: *AIAA/AAS Astrodynamics Specialist Conference*. American Institute of Aeronautics and Astronautics, Aug. 2012. DOI: 10.2514/6.2012-4435.

[12] Sanjay Talole, Joel Benito, and Kenneth Mease. “Sliding Mode Observer for Drag Tracking in Entry Guidance”. In: *AIAA Guidance, Navigation and Control Conference and Exhibit*. American Institute of Aeronautics and Astronautics, Aug. 2007. DOI: 10.2514/6.2007-6851.

[13] Marco Sagliano, Erwin Mooij, and Stephan Theil. “Adaptive Disturbance-Based High-Order Sliding-Mode Control for Hypersonic-Entry Vehicles”. In: *Journal of Guidance, Control, and Dynamics* (2016), pp. 1–16.

[14] Ping Lu. “Regulation about time-varying trajectories - Precision entry guidance illustrated”. In: *Guidance, Navigation, and Control Conference and Exhibit*. American Institute of Aeronautics and Astronautics, Aug. 1999. DOI: 10.2514/6.1999-4070.

[15] Carlo Alberto Pascucci, Samir Bennani, and Alberto Bemporad. “Model predictive control for powered descent guidance and control”. In: *2015 European Control Conference (ECC)*. IEEE, July 2015. DOI: 10.1109/ecc.2015.7330732.

[16] Youeyun Jung and Hyochoong Bang. “Mars precision landing guidance based on model predictive control approach”. In: *Proceedings of the Institution of Mechanical Engineers, Part G: Journal of Aerospace Engineering* 230.11 (Oct. 2015), pp. 2048–2062. DOI: 10.1177/0954410015607893.

[17] Keith Glover and John C. Doyle. “State-space formulae for all stabilizing controllers that satisfy an H∞-norm bound and relations to relations to risk sensitivity”. In: *Systems & Control Letters* 11.3 (Sept. 1988), pp. 167–172. DOI: 10.1016/0167-6911(88)90055-2.

[18] Ian Postlethwaite Sigurd Skogestad. *Multivariable Feedback Control*. John Wiley & Sons, Oct. 26, 2005. 592 pp. ISBN: 0470011688. URL: https://www.ebook.de/de/product/4018242/sigurd_skogestad_ian_postlethwaite_multivariable_feedback_control.html.

[19] J. Doyle. “Guaranteed margins for LQG regulators”. In: *IEEE Transactions on Automatic Control* 23.4 (Aug. 1978), pp. 756–757. DOI: 10.1109/tac.1978.1101812.

[20] J. Doyle, A. Packard, and K. Zhou. “Review of LFTs, LMIs, and mu”. In: *[1991] Proceedings of the 30th IEEE Conference on Decision and Control*. IEEE. DOI: 10.1109/cdc.1991.261572.

[21] Mathworks. *hinfsyn: Compute H-infinity optimal controller*. Retrieval Date: 09-Mar-2020. URL: https://mathworks.com/help/robust/ref/hinfsyn.html.

[22] *Control of Linear Parameter Varying Systems with Applications*. Springer-Verlag GmbH, Mar. 14, 2012. ISBN: 1461418321. URL: https://www.ebook.de/de/product/16338251/control_of_linear_parameter_varying_systems_with_applications.html.

[23] P. Apkarian and D. Noll. “Frequency Domain $H_\infty$ Synthesis using Nonsmooth Techniques”. In: *2006 1ST IEEE Conference on Industrial Electronics and Applications*. IEEE, May 2006. DOI: 10.1109/iciea.2006.257082.

[24] Bong Wie, Wei Du, and Mark Whorton. "Analysis and Design of Launch Vehicle Flight Control Systems". In: *AIAA Guidance, Navigation and Control Conference and Exhibit*. American Institute of Aeronautics and Astronautics, Aug. 2008. DOI: 10.2514/6.2008-6291.

[25] D. Wei. "Dynamic modeling and ascent flight control of Ares-I Crew Launch Vehicle". PhD thesis. Iowa State University, 2010. URL: https://lib.dr.iastate.edu/etd/11540.

[26] M. Knoblauch, D. Saussie, and C. Berard. "Structured $H_\infty$ control for a launch vehicle". In: *2012 American Control Conference (ACC)*. IEEE, June 2012. DOI: 10.1109/acc.2012.6315181.

[27] David Saussie, Quentin Barbes, and Caroline Berard. "Self-scheduled and structured $H_\infty$ synthesis : A launch vehicle application". In: *2013 American Control Conference*. IEEE, June 2013. DOI: 10.1109/acc.2013.6580062.

[28] M. Ganet-Schoeller and Jean Desmariaux. "Structured H∞ synthesis for flexible launcher control". In: *IFAC-PapersOnLine* 49.17 (2016), pp. 450–455. DOI: 10.1016/j.ifacol.2016.09.077.

[29] Diego Navarro-Tapia et al. "Structured H-infinity control based on classical control parameters for the VEGA launch vehicle". In: *2016 IEEE Conference on Control Applications (CCA)*. IEEE, Sept. 2016. DOI: 10.1109/cca.2016.7587818.

[30] Diego Navarro-Tapia et al. "Legacy recovery and robust augmentation structured design for the VEGA launcher". In: *International Journal of Robust and Nonlinear Control* 29.11 (Apr. 2019), pp. 3363–3388. DOI: 10.1002/rnc.4557.

[31] Diego Navarro-Tapia. "Robust and Adaptive TVC Control Design Approaches for the VEGA Launcher". PhD thesis. University of Bristol, 2019. URL: https://research-information.bris.ac.uk/en/theses/robust-and-adaptive-tvc-control-design-approaches-for-the-vega-launcher(3dd9fe89-58c1-47ae-9f94-f52b6e601cfa).html.

[32] Pedro Simplicio, Andres Marcos, and Samir Bennani. "New Control Functionalities for Launcher Load Relief in Ascent and Descent Flight". Eng. In: *8th European Conference for Aeronautics and Aerospace Sciences (EUCASS)* 8th European Conference for Aeronautics and Aerospace Sciences (EUCASS) (July 2019). DOI: 10.13009/EUCASS2019-275.

[33] spacex.com. *Falcon 9 User's Guide*. Retrieval Date: 09-Mar-2020. URL: https://www.spacex.com/sites/spacex/files/falcon_users_guide_10_2019.pdf.

[34] Pascal Gahinet and Pierre Apkarian. "A linear matrix inequality approach toH∞ control". In: *International Journal of Robust and Nonlinear Control* 4.4 (1994), pp. 421–448. DOI: 10.1002/rnc.4590040403.

[35] P. Apkarian and D. Noll. "Nonsmooth H∞Synthesis". In: *IEEE Transactions on Automatic Control* 51.1 (Jan. 2006), pp. 71–86. DOI: 10.1109/tac.2005.860290.

[36] Herbert Werner. *Optimal and Robust Control*. Tech. rep. Retrieval Date: 03-March-2020. Technische Universität Hamburg-Harburg, 2014. URL: https://www.tuhh.de/t3resources/ics/PDFs/Opt_Robust_Ctrl/orc.pdf.